Multiscale permutation entropy for two-dimensional patterns

Cristina Morel, Anne Humeau-Heurtier

Pattern Recognition Letters
journal homepage: www.elsevier.com

Multiscale permutation entropy for two-dimensional patterns

Cristina Morel[a,b,**], Anne Humeau-Heurtier[b]

[a]ESTACA - Campus Ouest, F-53061 Laval Cedex 9, France
[b]Univ Angers, LARIS, SFR MATHSTIC, F-49000 Angers, France

ABSTRACT

Complexity measures are important to understand and analyze systems with one dimensional data. However, extension of these methods to images (two dimensional data) are much less usual. Bidimensional multiscale sample entropy (MSE_{2D}) has recently been proposed as a new complexity measure for texture evaluation. However, MSE_{2D} leads to undefined or unreliable values for small-sized textures and requires a long computation time. This is why we herein propose the bidimensional multiscale permutation entropy (MPE_{2D}) to evaluate the complexity of 2D patterns. MPE_{2D} is applied to different synthesized textures, to softwood samples, and to study the texture of breast histopathology images. The results show that MPE_{2D} is a valuable tool for texture analysis and that it is computationally noticeably faster than MSE_{2D}.

1. Introduction

In the field of signal processing, the analysis of time series' irregularity through entropy measures is now well established. The corresponding work has led to many papers in several kinds of applications, including biomedical time series (Costa et al., 2005) (Humeau-Heurtier et al., 2011) (Humeau-Heurtier et al., 2012), vibrations of rotary machines (Wu et al., 2012), electroseismic time series (Guzman-Vargas et al., 2008), and financial time series (Niu and Wang, 2015). This has become possible since the 1990's when Pincus introduced the approximate entropy measure (Pincus, 1991). Later, in 2000, Richman and Moorman proposed the sample entropy to overcome some of the approximate entropy limitations (Richman and Moorman, 2000). Another widely used entropy method is fuzzy entropy (Chen et al., 2009). Although sample entropy is slightly faster than fuzzy entropy, the latter is more consistent and less dependent on the data length. In 2002, Bandt and Pompe proposed the permutation entropy ($PerEn_{1D}$) to study time series complexity (Bandt and Pompe, 2002). $PerEn_{1D}$ relies on the comparison of neighboring values and has the advantage, over sample entropy, of being very fast (low computation time). Later, in 2005, the multiscale permutation entropy (MPE_{1D}) has been introduced to study the permutation entropy over different time scales (Aziz and Arif, 2005). More recently, extensions to the 2D case of some of these measures have been developed to analyze image texture (Yeh et al., 2011), (Ribeiro et al., 2012), (Moore, 2016), (Silva et al., 2016), (Azami et al., 2017), (dos Santos et al., 2018), (Humeau-Heurtier et al., 2018), (Silva et al., 2018), (Azami et al., 2019), (Hilal et al., 2020). Thus, the bidimensional version of the sample entropy ($SampEn_{2D}$) and its spatial multiscale approach (MSE_{2D}) have been developed (Silva et al., 2018), (Humeau-Heurtier et al., 2018). The bidimensional version of the permutation entropy ($PerEn_{2D}$) has also been proposed (Ribeiro et al., 2012). In the latter work, the authors used the complexity-entropy causality plane and showed it can be useful to, among others, distinguish between two-dimensional patterns (Ribeiro et al., 2012), (Sigaki et al., 2018). This plane has also been used with a multiscale approach to discriminate image textures (Zunino and Ribeiro, 2016).

Our goal herein is to study the multiscale $PerEn_{2D}$ (MPE_{2D}) and to evaluate how it is able to differentiate textures. Our work is therefore different from the above-mentioned studies as no complexity-entropy causality plane is used. We rely only on $PerEn_{2D}$ and MPE_{2D} for texture analysis. Moreover, we compare our results with the ones obtained with $SampEn_{2D}$ and MSE_{2D}. For this, we first present $PerEn_{2D}$ and MPE_{2D} in Section 2. Section 3 presents the dataset we used: periodic and synthesized textures, vision textures, softwood images, and

**Corresponding author: Cristina Morel
e-mail: Cristina.MOREL@estaca.fr (Cristina Morel)

medical textures. Then, in Section 4, the results are detailed and discussed. We end with a Conclusion in Section 5.

2. Bi-dimensional multiscale permutation entropy

As mentioned above, the bidimensional multiscale sample entropy (MSE_{2D}) has been proposed as a new texture algorithm (Silva et al., 2018) (Humeau-Heurtier et al., 2018). It relies on a coarse-graining procedure and has shown interesting results for texture classification. The permutation entropy, initially proposed for one dimensional data ($PerEn_{1D}$) (Bandt and Pompe, 2002), has recently been generalized to two or higher-dimensional structures such as images: $PerEn_{2D}$ (Ribeiro et al., 2012) (Sigaki et al., 2018). Based on this, Zunino *et al.* proposed the multiscale two-dimensional complexity-entropy causality plane for image texture discrimination; their multiscale approach relies on embedding delays (Zunino and Ribeiro, 2012, 2016). However, no extension to several scales of the bidimensional permutation entropy MPE_{2D} using a multiscale coarse-graining-based approach exists. We therefore present herein a new bidimensional multiscale approach for texture analysis, MPE_{2D}. The computational steps for MPE_{2D} are detailed below. MPE_{2D} can be calculated for any image $\mathbf{x}$ represented by a matrix. The multiscale procedure decreases the two-dimensional array $\mathbf{x}$ with scale factor τ to a new two-dimensional reduced array $\mathbf{y}$. Following the encoding scheme introduced by Bandt and Pompe (Bandt and Pompe, 2002), the MPE_{2D} algorithm is defined with the following two steps:

- The coarse-graining procedure: the coarse-graining $2D$ procedure of an arbitrary image $\mathbf{x}$ with W width and H height, is defined by:

$$\mathbf{y}_{i,j}^{(\tau)} = \frac{1}{\tau^2} \sum_{\substack{k=(i-1)\tau+1 \\ l=(j-1)\tau+1}}^{\substack{k=i\tau \\ l=j\tau}} \mathbf{x}_{k,l}, \tag{1}$$

  where $1 \leq i \leq \lfloor H/\tau \rfloor$, $1 \leq j \leq \lfloor W/\tau \rfloor$ and τ is the scale factor. The coarse-grained image has the width $n_w = \lfloor W/\tau \rfloor$ and the height $n_h = \lfloor H/\tau \rfloor$. If the scale factor τ is equal to one, the coarse-grained image $\mathbf{y}^{(1)}$ corresponds to the original image $\mathbf{x}$.

- Application of $PerEn_{2D}$ on each coarse-grained image: this second step will be introduced by an example. Let us assume that the coarse-grained image is:

$$\mathbf{A} = \begin{pmatrix} 2 & 4 & 9 \\ 1 & 5 & 3 \\ 7 & 8 & 6 \end{pmatrix}. \tag{2}$$

  This second step relies on four parameters: the embedding dimensions d_x and d_y (d_x, $d_y \in N$), which split the initial matrix $\mathbf{A}$ into sub-matrices of size $d_x \times d_y$, and the embedding delays τ_x and τ_y (τ_x, $\tau_y \in N$), which define the spatial separation in horizontal and vertical directions, respectively. For instance, choosing $d_x = d_y = 2$ leads to the first partition $d_x \times d_y$ of the initial matrix $\mathbf{A}$:

$$\mathbf{A}_1 = \begin{pmatrix} 2 & 4 \\ 1 & 5 \end{pmatrix} = \begin{pmatrix} a_0 & a_1 \\ a_2 & a_3 \end{pmatrix}, \tag{3}$$

  which is, after a reshaping step, (2415). It is clear that this $2D$ partition or the sub-matrix $\mathbf{A}_1$ becomes a one-dimensional data. The smaller element of this one-dimensional data is 1, which corresponds to the element a_2. We hold the index 2. The next element larger than a_2 is 2, giving the element a_0, so the index is 0. For 4 and 5, the elements are a_1 and a_3, so the indices 1 and 3 are obtained. This sub-matrix leads to the elements $a_2 \leq a_0 \leq a_1 \leq a_3$ in ascending order after sort. Then, the indices of the terms a_i, ($0 \leq i \leq 3$), determine the state (2013). The second partition is defined as a matrix $d_x \times d_y$, offset by $\tau_x = 1$, in the horizontal direction. This partition:

$$\mathbf{A}_2 = \begin{pmatrix} 4 & 9 \\ 5 & 3 \end{pmatrix} \rightarrow \underbrace{(4\,9\,5\,3)}_{reshape} \tag{4}$$

  is composed of the elements (4953), after a reshaping step. Putting the matrix elements a_0, a_1, a_2, a_3, in ascending order $a_3 \leq a_0 \leq a_2 \leq a_1$, gives the index of the matrix elements are mapped to the ordinal pattern (3021). The third sub-matrix

$$\mathbf{A}_3 = \begin{pmatrix} 1 & 5 \\ 7 & 8 \end{pmatrix} \tag{5}$$

  leads to the state (0123) due to the offset by $\tau_y = 1$, on the vertical direction. With $\tau_x = 1$ and $\tau_y = 1$, the last remaining sub-matrix

$$\mathbf{A}_4 = \begin{pmatrix} 5 & 3 \\ 8 & 6 \end{pmatrix}, \tag{6}$$

  leads to the ordinal pattern (1032). However, by changing the embedding delays $\tau_x = 2$ on the horizontal direction and $\tau_y = 1$ on the vertical direction, the elements in the original matrix are non-consecutive. In this case, two partitions with their permutations are obtained from the array $\mathbf{A}$:

$$\mathbf{A}_5 = \begin{pmatrix} 2 & 9 \\ 1 & 3 \end{pmatrix} \rightarrow \underbrace{(2\,9\,1\,3)}_{reshape} \tag{7}$$

  leads to (2031) and

$$\mathbf{A}_6 = \begin{pmatrix} 1 & 3 \\ 7 & 6 \end{pmatrix} \rightarrow \underbrace{(1\,3\,7\,6)}_{reshape} \tag{8}$$

  leads to (0132). The parameters d_x and d_y determine the number of accessible states: they play an important

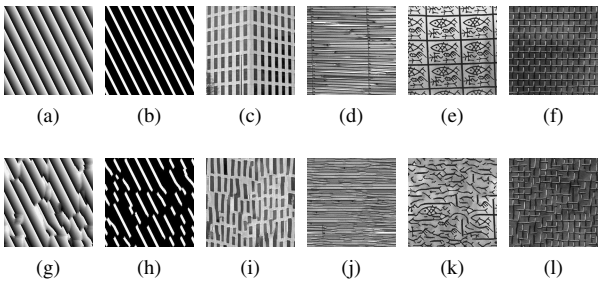

Fig. 1. Six examples of texture synthesis: (a) to (f) are periodic textures and (g) to (l) are the corresponding synthetic textures (in the same order).

role in the estimation of the permutation probability distribution P. It is usual to choose $d_x! \ll W$ for the one-dimensional case (Bandt and Pompe, 2002); for the two-dimensional case, a similar relationship is recommended, i.e. $(d_x \times d_y)! \ll W \times H$.

The probability distribution $P = \{p_i; i = 1, \ldots, (d_x \times d_y)!\}$ is obtained by computing the frequencies of the possible patterns relative to $(d_x \times d_y)!$. Having the probability distribution, the normalized Shannon entropy is calculated as

$$H(p) = -\frac{1}{\ln((d_x \times d_y)!)} \sum_{i=0}^{(d_x \times d_y)!} p_i \times \ln p_i. \quad (9)$$

Therefore, if the pixels of an image represented by a matrix are highly disordered, the value of the normalized Shannon entropy is near to one; on the contrary, the normalized Shannon entropy is near to zero if they always appear in the same order. It is important to note that the coarse-graining approach is performed before the computation of $PerEn_{2D}$. This means that for an original image of size 50×50 pixels at scale factor $\tau = 5$, we obtain first a coarse-grained image of 10×10 pixels, which then leads to a 100 samples time series.

3. Datasets

In this section, we briefly describe the different synthesized and real-life textures used to study MPE_{2D} behavior.

3.1. Artificial periodic and synthesized textures

We first studied MPE_{2D} behavior for six periodic textures and their corresponding synthesized textures. These images are from the database `https://graphics.stanford.edu/projects/texture/demo/synthesis_eero.html`. The original textures, sized 256×256 pixels, are depicted in Fig. 1(a) to (f). The corresponding synthesized textures are shown in Fig. 1(g) to (l). The synthesis algorithm is based on Markov random field texture models. It generates textures through a deterministic search process (Wei and Levoy, 2000). Each local region of the synthesized texture based on this algorithm is similar to another region from the input (original periodic) texture.

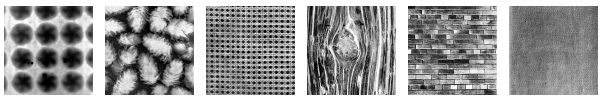

Fig. 2. Vision textures ordered from the least irregular (a) to the most irregular (f).

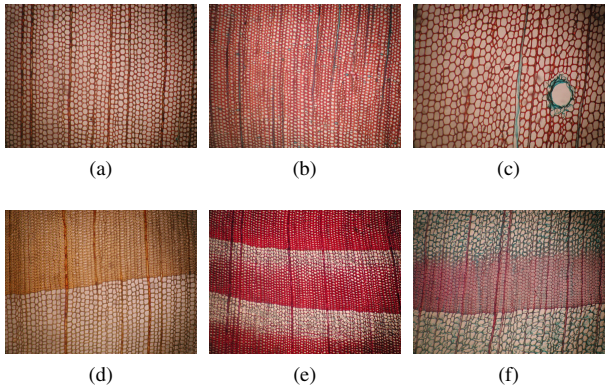

Fig. 3. Softwood cross section: (a) Cupressus lindleyi, (b) Podocarpus lambertii, (c) Pinus caribaea, (d) Pseudotsuga macrolepsis, (e) Tsuga sp, (f) Larix lariciana.

3.2. Vision textures

To study MPE_{2D} for different irregular textures, we processed six vision textures from `https://multibandtexture.recherche.usherbrooke.ca/normalized_brodatz.html`. The textures, sized 640 × 640 pixels, are shown in Fig. 2(a) to (f), ordered from the least irregular to the most irregular.

3.3. Softwood textures

We evaluated MPE_{2D} to measure the complexity of some softwood species. The database (`http://web.inf.ufpr.br/vri/databases/forest-species-database-microscopic/`) contains 112 different forest species which were cataloged by the Laboratory of Wood Anatomy at the Federal University of Parana in Curitiba, Brazil. The microscopic images have been acquired and carefully labeled by experts in wood anatomy. Fourteen softwood species were collected at random from the database (Abies religiosa, Cedrus atlantica and sp (Aussenac, 1984), Cupressus arizonica, Cupressus lindleyi (Richter et al., 2004), Larix lariciana, Pinus caribaea, Pinus maximinoi (Martins et al., 2013), Podocarpus lambertii, Pseudotsuga macrolepsis, Sequoia sempervirens (Martins et al., 2013), Taxodium distichum, Torreya nucifera, Tsuga sp (Martins et al., 2013)). Figure 3 presents some softwood species. There are 280 samples used in the experiment, 20 images for each of the 14 species, with a resolution of 1024 × 768 pixels. All these images can be divided into two groups (uniform transitions and gradual transitions), as described below.

Softwoods (coniferous trees) produce a single cell type, the tracheid. The conifers growing under tropical (Chattaway, 1934) conditions are characterized by a relatively uniform

cross-sectional structure composed of tracheids with similar diameters and thicknesses of walls, such as Cupressus lindleyi (Fig. 3 (a)), Podocarpus lambertii (Fig. 3 (b)), and Pinus caribaea (Fig. 3 (c)). This kind of conifer has a uniform transition from the earlywood (faster-growing wood) to the latewood (slower-growing wood). Because of the wet climate where growing conditions are similar year round, distinct annual growth rings boundaries may be absent or indistinct, as for example Podocarpus lambertii or Taxodium distichum.

In regions of the world where climate is distinctly seasonal, with long cold periods that halt tree growth, there can be a gradual increase in wall thickening near the end of the growth ring. The conifers develop thin-walled tracheids in the earlywood and smaller-diameter tracheids with thick-walled in the latewood. This transition from the earlywood to the latewood can be very gradual for Pseudotsuga macrolepsis (Fig. 3 (d)), Tsuga sp (Fig. 3 (e)), Larix lariciana (Fig. 3 (f)) or very abrupt for Sequoia sempervirens.

3.4. Medical images

We also evaluated MPE_{2D} on medical images. We thus studied pathological and healthy tissues in breast medical images. We used the database (`https://www.kaggle.com/paultimothymooney/breast-histopathology-images`). In this database, the patients are diagnosed clinically having a breast cancer disease. Breast cancer is the most common form of cancer for women, and invasive ductal carcinoma is the most common form of breast cancer. Accurately, identifying and categorizing breast cancer types is an important clinical task, to save time and reduce error. This database consists of images of breast cancer scanned at $40x$, issued from 279 subjects. From that, 277524 patches of 50×50 pixels were extracted, with 198738 benign tissue patches (negative) and 78786 malignant tissue patches (positive to presence of invasive ductal carcinoma cancer). For our experiment, we selected 50 subjects and 270 patches for each subject (i.e. 13500 patches), with a resolution of 50×50 pixels.

4. Results and discussion

For the all the results presented below, d_x and d_y were set to 2, and τ_x and τ_y were set to 1.

4.1. Artificial periodic and synthesized textures

In order to study the multiscale approach on $PerEn_{2D}$, we used different values of the scale factor τ: 1 to 10. Moreover, based on (Costa and Goldberger, 2015) and (Zhang, 1991), we computed a complexity index computed as the mean of the $PerEn_{2D}$ values over scale factors 1 to 10. Figures 4(a) to (f) show MPE_{2D} of the periodic textures represented on Figs. 1(a) to (f) and of the corresponding synthetic textures represented on Figs. 1(g) to (l) (in the same order). For all six images of Figs. 1(a) to (f), MPE_{2D} of the periodic texture is lower over all the scales τ than the one of the synthesized texture, as shown in Figs. 4(a) to (f). This is also shown in Tables 1 and 2.

The same results are obtained for the mean of MSE_{2D}: the mean of MSE_{2D} of all periodic textures is lower than for synthesized textures, see Tables 1 and 2. This shows that both

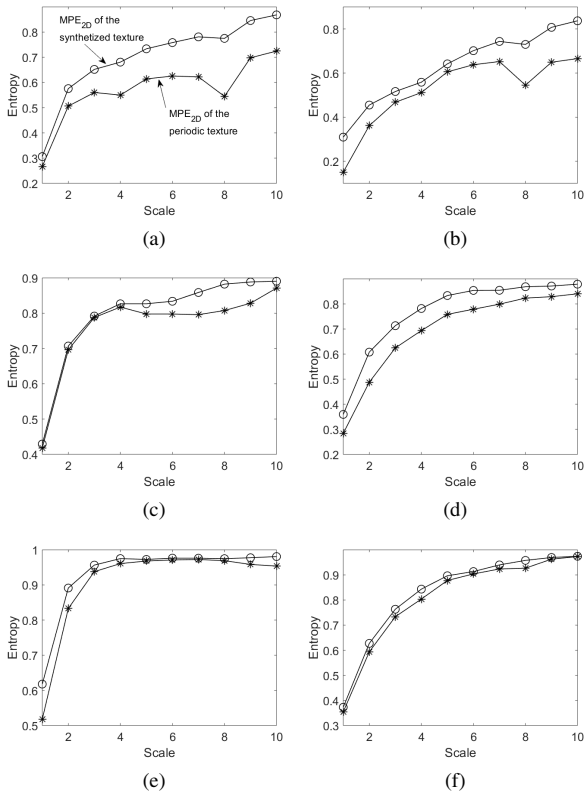

Fig. 4. MPE_{2D} **computed for texture synthesis examples: periodic textures and the corresponding synthesized textures; see Fig. 1 for details.**

Table 1. The mean of MPE_{2D} and the mean of MSE_{2D} of the periodic textures, see Fig. 1, over all scale factors τ from 1 at 10 and their computation time in seconds.

	(a)	(g)	(b)	(h)	(c)	(i)
MPE_{2D}	0.57	0.69	0.52	0.63	0.76	0.79
Duration	0.88	0.74	0.88	0.75	0.87	0.73
MSE_{2D}	0.28	2.81	1.44	2.06	2.58	2.95
Duration	47.62	45.91	55.78	58.08	44.69	46.53

Table 2. The mean of MPE_{2D} and the mean of MSE_{2D} of the synthetic textures, see Fig. 1, over all scale factors τ from 1 at 10 and their computation time in seconds.

	(d)	(j)	(e)	(k)	(f)	(l)
MPE_{2D}	0.69	0.76	0.89	0.93	0.80	0.82
Duration	0.83	0.81	0.88	0.75	0.89	0.79
MSE_{2D}	2.4	2.98	2.73	4.38	1.85	2.37
Duration	58.82	56.78	48.31	50.54	68.25	70.01

MPE_{2D} and MSE_{2D} may be of interest to properly discriminate periodic from synthesized textures by assigning lower entropy values for periodic textures (highly ordered textures).

The computation times for MPE_{2D} and MSE_{2D} are shown in Tables 1 and 2. The simulations have been carried out using a PC with $Intel\ (R)\ Core(TM)\ i5-7200U\ CPU, 2.5\ GHz$ and $8GB\ RAM$ by $Matlab\ R2018b$. MPE_{2D} is about 100 times faster than MSE_{2D} for this image size.

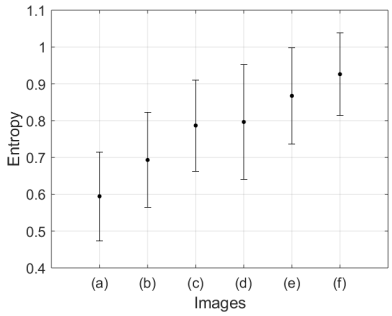

Fig. 5. Mean and standard deviation of MPE_{2D} for scale factors $\tau = 1$ to 10 for vision textures ordered from the least irregular (a) to the most irregular (f); see Fig. 2.

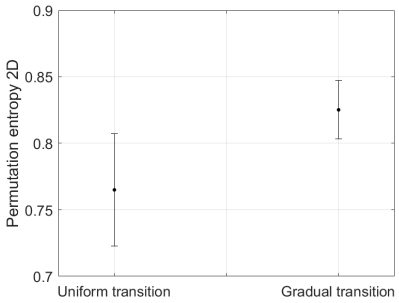

Fig. 6. Mean and standard deviation of MPE_{2D} computed for 280 softwood samples images: uniform transition, tracheids with similar diameters and thicknesses of the walls, specific to the tropical forests, and gradual transition for temperate regions, with thin and thick-walled tracheids.

Table 3. The mean of MPE_{2D} and the mean of MSE_{2D} of the vision textures, see Fig. 2, over all scale factors τ from 1 at 10 and their computation time in seconds.

	(a)	(b)	(c)	(d)	(e)	(f)
MPE_{2D}	0.59	0.69	0.78	0.79	0.86	0.93
Duration	0.51	0.47	0.46	0.47	0.48	0.51
MSE_{2D}	2.04	3.08	3.34	3.88	3.89	4.11
Duration	2345	2230	2282	2041	2224	2196

Table 4. The mean of MPE_{2D} of the softwood species over all scale factors τ from 1 at 10. TkW refers to thick-walled tracheids and TnW refers to thin-walled tracheids.

Species	MPE_{2D}	Tracheids
Abies religiosa	0.84	TnW and TkW
Cedrus atlantica	0.85	TnW and TkW
Cedrus sp.	0.86	TnW and TkW
Cupressus arizonica	0.77	similar diameters
Cupressus lindleyi	0.77	similar diameters
Larix lariciana	0.87	TnW and TkW
Pinus caribaea	0.74	similar diameters
Pinus maximinoi	0.84	TnW and TkW
Podocarpus lambertii	0.78	similar diameters
Pseudotsuga macrolepsis	0.84	TnW and TkW
Sequoia sempervirens	0.66	similar diameters
Taxodium distichum	0.77	similar diameters
Torreya nucifera	0.77	similar diameters
Tsuga sp.	0.85	TnW and TkW

4.2. Vision textures

The mean of MPE_{2D} over all scales (scale factors τ from 1 to 10) is in increasing order for the vision textures represented in Fig. 2, from the least irregular to the most irregular, see Fig. 5. As for the previous example, the comparison of the mean of MPE_{2D} and the mean of MSE_{2D} is presented in Table 3. We observe that the values increase as the irregularity of the texture increases.

At the same time, the MSE_{2D} method simulation time is around 4000 times larger than the one of MPE_{2D}.

4.3. Softwood textures

Recently, computer vision has been used to classify forest species. Tou *et al.* (Tou et al., 2007), proposed a computer vision-based wood recognition system using Gray Level Co-occurrence Matrix (GLCM) to extract texture features and neural network. Khalid *et al.* (Khalid et al., 2008) have developed an automatic Tropical Wood Species Recognition System for the classification of 20 different tropical Malaysian wood species using Multilayer Perceptron Backpropagation Artificial Neural Network as classifier. Yusof *et al.* (Yusof et al., 2010) offered a recognition system approach for the tropical wood species using Gabor filter, GLCM with multilayer perceptron back-propagation. Wang *et al.* (Wang et al., 2010) presented a wood recognition approach using Gabor wavelet coefficients. Cavalin *et al.* (Cavalin et al., 2013) proposed a system to classify 112 Brazilian forest species using multiple feature vectors based on Local binary patterns, GLCM and Linear phase quantization. Khairuddin *et al.* (Khairuddin et al., 2011) used feature selection based on genetic algorithm to improve the accuracy of wood species recognition.

Due to the large variations of features among the species of the tropical wood, and the problems related to variations in the wood samples, it is important to improve the methodology of the wood recognition system. Therefore, in this paper, we propose to compute MPE_{2D} over all scale factors $\tau = 1$ to 10, for the 14 softwood species, each one including 20 images per species. Table 4 presents the mean of MPE_{2D} for each softwood species and theirs tracheids. Figure 6 presents the mean and the standard deviation of MPE_{2D} for the softwood. For all conifers growing under wet conditions, see Table 4 (Cupressus arizonica, Cupressus lindleyi, Pinus caribaea, Podocarpus lambertii, Sequoia sempervirens, Taxodium distichum, Torreya nucifera), the value of the mean of MPE_{2D} is 0.76 and the standard deviation is lower than 0.04. In temperate regions of the world, these conifers develop different diameter tracheids with different walled tracheids leading to a higher complexity. The mean of MPE_{2D} for Abies religiosa, Cedrus atlantica, Cedrus sp, Pinus maximinoi, Pseudotsuga macrolepsis (Fig. 3 (d)), Tsuga sp (Fig. 3 (e)) and Larix lariciana (Fig. 3 (f)) is 0.83 and the standard deviation is lower than 0.02.

It is well know that the thinner walls are found in more humid environments, and the thicker walls are associated with drier environments (Ramagea et al., 2017), (Alves and Angyalossy-Alfonso, 2002). Rapid or constant growing wood in the tropics leads to large cells with thinner walls allowing for efficient wa-

Table 5. p**-values obtained with the Mann-Whitney test on Haralick features for the two following groups: 1) uniform transition, tracheids with similar diameters and thicknesses of the walls, specific to the tropical forests (7 wood species; mean features computed from 20 images for each species); 2) gradual transition for temperate regions, with thin and thick-walled tracheids (7 wood species; mean features computed from 20 images for each species).** d **represents the interpixel distances for the co-occurrence matrices.**

Softwood textures	$d = 1$	$d = 2$	$d = 3$	$d = 4$
Contrast	1	1	0.9015	0.8048
Variance	0.1282	0.0973	0.1282	0.1282
Entropy	0.6200	0.6200	0.3829	1
Homogeneity	0.0728	0.0262	0.0530	0.1282
Correlation	0.2593	0.4557	0.3829	0.2086

ter transport to support intense photosynthesis. In temperate regions of the world, the slower or stoping growing wood in winter is characterized by more dense and smaller cells. So, the tropical species developed uniform cross-sectional structure with a repetitive appearance which leads to lower MPE_{2D}, whereas the temperate species develop a gradual cross-sectional structure with much more complex appearance leading to larger values of MPE_{2D}.

The Mann-Whitney test used to compare the values of the two groups of wood (the thick and the thin-walled fibres of the cross-sectional structure of the softwood) returns $p < 0.05$ ($p = 2.33 \times 10^{-3}$). This shows that MPE_{2D} values of the two groups of wood are statistically significantly different. We also compared our results with Haralick features from 2D co-occcurrence matrices. The p-values obtained with the Mann-Whitney test are shown in Table 5. We observe that MPE_{2D} surpasses the results given by Haralick features as the p-value given by the former method is lower than those given by the latter method.

4.4. Medical images

The database used in this work contains different patches. Each patch's file name includes the identity number of the patient, the x and y coordinates of the point where the patch was cropped from and the pathological and the healthy group. According to the x and y coordinates of the patch with 50×50 pixels resolution, the patches were put one after the other and one under the other, generating an image with a 150×150 pixels resolution (see Fig. 7). This has been performed because, choosing images as small as 50×50 pixels and using scale factors going from 1 to 10 would have lead to so short vectors that the permutation entropy values would have been erroneous. For images with a 50×50 pixels resolution, after a reshaping step, the time series would have had 2500 samples (τ =1). For $\tau = 10$, the time series would have been reduced to 25 samples. Tests on white noise images have shown that for images sizes larger than 150×150 pixels and for scale factors between 1 and 10, no such errors are observed (data not shown here). The database used in this experiment consists of 13500 patches of 50×50 pixels resolution to generate 1500 images of 150×150 pixels resolution.

From the database we selected randomly 50 subjects with the following identities: 8863, 8864, 8917, 8956, 8974, 8975, 9077, 9126, 9173, 9176, 9177, 9226, 9250, 9255, 9256, 9320, 9323, 9324, 9345, 9346, 9382, 10260, 10264, 10273, 10292, 10299, 10303, 10308, 12242, 12749, 12751, 12752, 12818, 12867, 12880, 12895, 12900, 12907, 13693, 14079, 14154, 14157, 14191, 14211, 15473, 15510, 15902, 16165, 16166, 16568. For each subject, we computed 15 images of size 150×150 pixels with benign tissues and 15 images of size 150×150 pixels with malignant tissues (see Fig. 8).

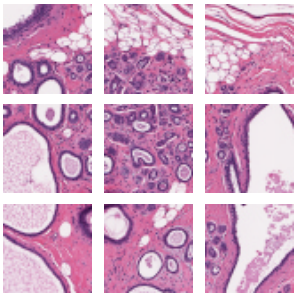

Fig. 7. Example of patch images used in the experiment for the subject id 10260**: 9 normal tissue patches without cancer.**

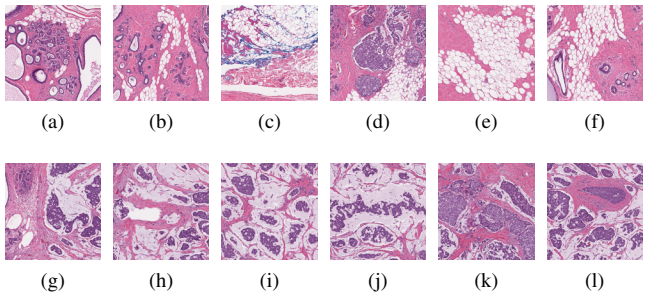

Fig. 8. Twelve examples of patch images of size 150×150 **pixels obtained from subject id.** 10260**: (a) to (f) benign tissues and (g) to (l) malignant tissues.**

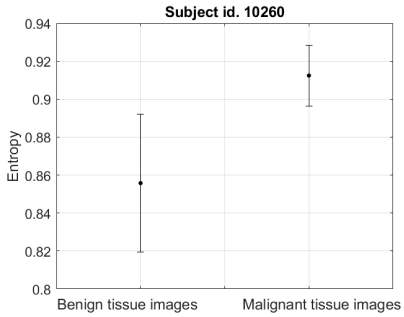

Fig. 9. Mean and standard deviation of MPE_{2D} **computed from scale factors** τ = 1 **to** 10 **for subject id.** 10260**. The results have been computed from** 15 **images of benign tissues and** 15 **images of malignant tissues (size of each image:** 150×150 **pixels).**

Figure 9 shows the mean and standard deviation for MPE_{2D} computed for scale factors $\tau = 1$ to 10 for subject id. 10260. For this subject, the mean of MPE_{2D} of the benign tissues is 0.856, with 0.036 for the standard deviation. For the malignant tissues, the mean of the MPE_{2D} is 0.912, with a standard deviation of 0.016. The results show that the mean of MPE_{2D} of all 15 benign tissues is lower to the mean of MPE_{2D} of all 15 malignant tissues.

Let us now use images from another subject (subject id.

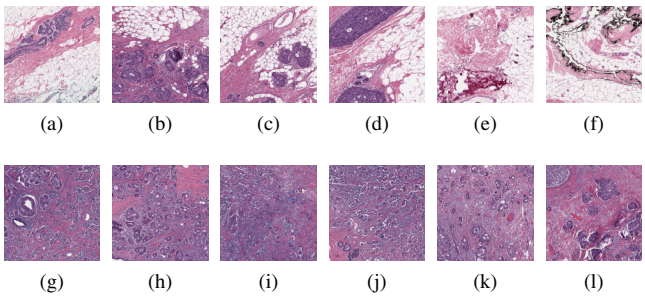

Fig. 10. Twelve examples of patch images of size 150×150 **pixels obtained from subject id.** 9320**: (a) to (f) benign tissues and (g) to (l) malignant tissues.**

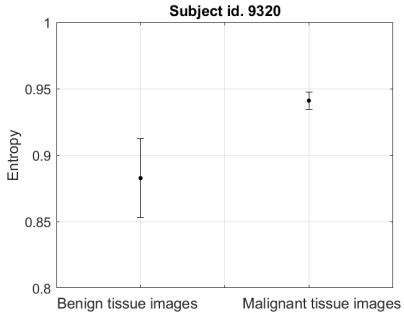

Fig. 11. Mean and standard deviation of MPE_{2D} computed from scale factors τ = 1 to 10 **for subject id.** 9320**. The results have been computed from** 15 **images of benign tissues and** 15 **images of malignant tissues (size of each image :** 150×150 **pixels).**

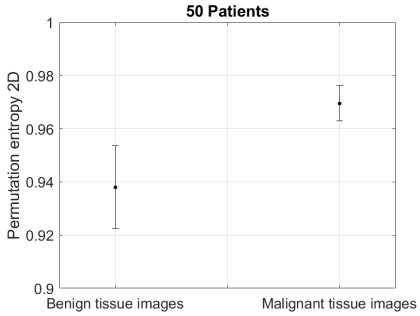

Fig. 12. Mean and standard deviation of MPE_{2D} computed from scale factors τ = 1 to 10 **for** 50 **subjects. The results have been computed from** 750 **images of benign tissues and** 750 **images of malignant tissues (size of each image :** 150×150 **pixels).**

Table 6. p-values obtained with the Wilcoxon signed rank test on Haralick features for two group: benign tissues (50 subjects, mean features computed from 15 images for each subject) and malignant tissues (50 subjects, mean features computed from 15 images for each subject). d represents the interpixel distances for the co-occurrence matrices.

Medical images	$d = 1$	$d = 2$	$d = 3$	$d = 4$
Contrast	1.645×10^{-1}	4.675×10^{-2}	1.069×10^{-1}	8.752×10^{-2}
Variance	8.435×10^{-8}	1.044×10^{-7}	1.160×10^{-7}	1.223×10^{-7}
Entropy	2.536×10^{-4}	3.757×10^{-5}	4.260×10^{-4}	7.563×10^{-5}
Homogeneity	2.257×10^{-5}	6.250×10^{-6}	6.250×10^{-6}	5.972×10^{-6}
Correlation	1.143×10^{-6}	9.397×10^{-7}	1.457×10^{-6}	1.089×10^{-6}

9320). Figure 10 presents 6 of the 15 benign and 6 of the 15 malignant tissue images. Each set of images is homogeneous, but the two sets have different structures. The mean of MPE_{2D} of the benign tissues is 0.883, with 0.029 for the standard deviation. For the malignant tissues, the mean of MPE_{2D} is 0.941, with a standard deviation of 0.0065, see Fig. 11. As for the case above, the mean of MPE_{2D} of all 15 benign tissues is lower than the mean of MPE_{2D} of all 15 malignant tissues.

On the same way, MPE_{2D} has been computed for the 50 subjects to categorize benign and the malignant tissues. The mean and the standard deviation for these 50 subjects (leading to 750 benign tests and 750 malignant tests) are represented in Fig. 12. As shown in this figure, the benign tissues have a mean MPE_{2D} of 0.9380 while the malignant tissues have a mean MPE_{2D} of 0.9695.

A Wilcoxon signed rank test between the two groups of tissues returns a p-value of $p = 7.79 \times 10^{-10}$, suggesting that the difference between the two groups is significant. We also compared our results with Haralick features from 2D co-occurrence matrices. The p-values obtained with the Wilcoxon signed rank test are shown in Table 6. We observe that MPE_{2D} surpasses the results given by Haralick features as the p-value given by the former method is lower than those given by the latter method.

4.5. Advantages and limitations

Entropy measures allow the quantification of irregularity, unpredictability or uncertainty. Considering that the repeatability of pixel patterns is related to the texture properties of images, $PerEn_{2D}$ can be considered as a meaningful feature extraction technique, representing characteristics related to the texture of images. The multiscale approach – that comes before the permutation entropy computation – allows to study the image at different spatial scale factors, which is an important step as images are often complex structures with different textures at small and large spatial scales.

Image irregularity and complexity can be useful for image characterization, and for any application using texture analysis such as remote sensing, assisted medical diagnosis, automatic target recognition, and for classification.

The advantage of MPE_{2D}, compared to other entropy methods, is its simplicity and extremely fast calculation. However, for time series, it has been shown that equal or repeated values can introduce a bias in the estimation of the ordinal pattern probability distribution when computing $PerEn_{1D}$ (Cuesta-Frau et al., 2018). Several attempts have been proposed to overcome this drawback for time series (Chen et al., 2019; Azami and Escudero, 2016; Bian et al., 2012; Bandt, 2005). This problem of equal values for permutation entropy applied to images has not been studied yet, from the best of our knowledge. If it really leads to errors in image classification, we could think of maximising the embedding dimension (Cuesta-Frau et al., 2018) or extending the above-mentioned studies dedicated to signals for images. However, as Cuesta-Frau *et al.* mentioned (Cuesta-Frau et al., 2018), the problem of ties in permutation entropy has been probably overrated when using permutation entropy for signal classification. This might be the same for images.

5. Conclusion

We introduced MPE_{2D} to quantify the complexity of image textures. The results show the ability of MPE_{2D} to distinguish periodic textures from synthesized textures, different types of softwood textured surfaces, and different textures of breast histopathologic images. MPE_{2D} is a valuable tool for texture analysis and is computationally noticeably faster than MSE_{2D}.

References

Alves, E., Angyalossy-Alfonso, V., 2002. Ecological trends in the wood anatomy of some brazilian species. 2. axial parenchyma, rays and fibres. IAWA Journal 23, 391–418.

Aussenac, G., 1984. Le cèdre, essai d'interprtation bioclimatique et écophysiologique. Bulletin de la Socit Botanique de France. Actualits Botaniques 131, 385–398.

Azami, H., Escudero, J., 2016. Amplitude-aware permutation entropy: Illustration in spike detection and signal segmentation. Computer Methods and Programs in Biomedicine 128, 40–51.

Azami, H., Escudero, J., Humeau-Heurtier, A., 2017. Bidimensional distribution entropy to analyze the irregularity of small-sized textures. IEEE Signal Processing Letters 24, 1338–1342.

Azami, H., da Silva, L.E.V., Omoto, A.C.M., Humeau-Heurtier, A., 2019. Two-dimensional dispersion entropy: An information-theoretic method for irregularity analysis of images. Signal Processing: Image Communication 75, 178–187.

Aziz, W., Arif, M., 2005. Multiscale permutation entropy of physiological time series, IEEE Pakistan Section Multitopic Conference. pp. 1–6.

Bandt, C., 2005. Ordinal time series analysis. Ecological Modelling 182, 229–238.

Bandt, C., Pompe, B., 2002. Permutation entropy: a natural complexity measure for time series. Physical Review Letters 88, 174102.

Bian, C., Qin, C., Ma, Q.D., Shen, Q., 2012. Modified permutation-entropy analysis of heartbeat dynamics. Physical Review E 85, 021906.

Cavalin, P., Kapp, M., Martins, J., Oliveira, L., 2013. A multiple feature vector framework for forest species recognition, Annual ACM Symposium on Applied Computing, New York, USA. p. 1620.

Chattaway, M., 1934. TROPICAL WOODS. School of Forestry.

Chen, W., Zhuang, J., Yu, W., Wang, Z., 2009. Measuring complexity using fuzzyen, apen, and sampen. Medical Engineering and Physics 31, 61–68.

Chen, Z., Li, Y., Liang, H., Yu, J., 2019. Improved permutation entropy for measuring complexity of time series under noisy condition. Complexity 2019, Article ID 1403829.

Costa, M., Goldberger, A., Peng, C., 2005. Multiscale entropy analysis of biomedical signals. Physical Review E 71, 021906.

Costa, M.D., Goldberger, A.L., 2015. Generalized multiscale entropy analysis: Application to quantifying the complex volatility of human heartbeat time series. Entropy 17, 1197–1203.

Cuesta-Frau, D., Varela-Entrecanales, M., Molino-Pico, A., Vargas, B., 2018. Patterns with equal values in permutation entropy: Do they really matter for biosignal classification? Complexity 2018, Article ID 1324696.

Guzman-Vargas, L., Ramirez-Rojas, A., Angulo-Brown, F., 2008. Multiscale entropy analysis of electroseismic time series. Natural Hazards and Earth System Sciences 8, 855–860.

Hilal, M., Berthin, C., Martin, L., Azami, H., Humeau-Heurtier, A., 2020. Bidimensional multiscale fuzzy entropy and its application to pseudoxanthoma elasticum. IEEE Transactions on Biomedical Engineering, in press .

Humeau-Heurtier, A., Mahe, G., Chapeau-Blondeau, F., Rousseau, D., Abraham, P., 2011. Multiscale analysis of microvascular blood flow: A multiscale entropy study of laser Doppler flowmetry time series. IEEE Transactions on Biomedical Engineering 58, 2970–2973.

Humeau-Heurtier, A., Mahe, G.Durand, S., Abraham, P., 2012. Multiscale entropy study of medical laser speckle contrast images. IEEE Transactions on Biomedical Engineering 60, 872–879.

Humeau-Heurtier, A., Omoto, A.C.M., Silva, L.E., 2018. Bi-dimensional multiscale entropy: Relation with discrete Fourier transform and biomedical application. Computers in Biology and Medicine 100, 36–40.

Khairuddin, U., Yusof, R., Khalid, M., 2011. Optimized feature selection for improved tropical wood species recognition system. ICIC International Journal of Research and Surveys, Express letters, Part B Applications 2, 441–446.

Khalid, M., Lee, E., Yusof, R., Nadaraj, M., 2008. Design of an intelligent wood species recognition system. International Journal of Simulation System, Science and Technology 9, 9–19.

Martins, J., Oliveira, L.S., Nisgoski, S., Sabourin, R., 2013. A database for automatic classification of forest species. Machine Vision and Applications 24, 567578.

Moore, C.J., 2016. A threshold structure metric for medical image interrogation: the 2d extension of approximate entropy., 20th IEEE International Conference Information Visualisation (IV). pp. 336–341.

Niu, H., Wang, J., 2015. Quantifying complexity of financial short-term time series by composite multiscale entropy measure. Communications in Nonlinear Science and Numerical Simulation 22, 375–382.

Pincus, S., 1991. Approximate entropy as a measure of system complexity. Proceedings of the National Academy of Sciences 88, 2297–2301.

Ramagea, M., Burridgeb, H., Busse-Wicherc, M., Feredaya, G., Reynoldsa, T., Shaha, D., Wud, G., Yuc, L., Fleminga, P., Densley-Tingleye, D., Allwoode, J., Dupreec, P., Lindenb, P., Schermane, O., 2017. The wood from the trees: The use of timber in construction. Renewable and Sustainable Energy Reviews 68, 333–359.

Ribeiro, H., Zunino, L., Lenzi, E., Santoro, P., Mendes, R., 2012. Complexity-entropy causality plane as a complexity measure for two-dimensional patterns. Plos ONE 7, 1–9.

Richman, J., Moorman, J., 2000. Physiological time-series analysis using approximate entropy and sample entropy. American Journal of Physiology-Heart and Circulatory Physiology 278, H2039–H2049.

Richter, H., Grosser, D., Heinz, I., Gasson, P., 2004. Iawa list of microscopic features for softwood identification. IAWA Journal 25, 1–70.

dos Santos, L.F.S., Neves, L.A., Rozendo, G.B., Ribeiro, M.G., do Nascimento, M.Z., Tosta, T.A.A., 2018. Multidimensional and fuzzy sample entropy (sampenmf) for quantifying h and e histological images of colorectal cancer. Computers in Biology and Medicine 103, 148–160.

Sigaki, H., Perc, M., Ribeiro, H., 2018. History of art paintings through the lens of entropy and complexity. Proceedings of the National Academy of Sciences 115, E8585E8594.

Silva, L., Duque, J., Felipe, J., Murta, L., Humeau-Heurtier, A., 2018. Two-dimensional multiscale entropy analysis: Applications to image texture evaluation. Signal Processing 147, 224–232.

Silva, L., Filho, A., Fazan, V., Felipe, J., Junior, L., 2016. Two-dimensional simple entropy: assessing image texture through irregularity. Biomedical Physics and Engineering Express 2, 045002.

Tou, J., Lau, P., Tay, Y., 2007. Computer vision-based wood recognition system, Proceedings of International Workshop on Advanced Image Technology.

Wang, B., Wang, H., Qi, H., 2010. Wood recognition based on greylevel co-occurrence matrix, International Conference on Computer Application and System Modeling. pp. 269–272.

Wei, L., Levoy, M., 2000. Fast texture synthesis using tree-structured vector quantization, Proceedings of the 27th annual conference on Computer graphics and interactive techniques, ACM Press/Addison-Wesley Publishing Co., 2000, pp. 479488.

Wu, S., Wu, P., Wu, C., Ding, J., Wang, C., 2012. Bearing fault diagnosis based on multiscale permutation entropy and support vector machine. Entropy 14, 1343–1356.

Yeh, J.R., Lin, C.W., Shieh, J.S., 2011. An approach of multiscale complexity in texture analysis of lymphomas. IEEE Signal Processing Letters 18, 239–242.

Yusof, R., Rosli, N., Khalid, M., 2010. Using gabor filters as image multiplier for tropical wood species recognition system, International Conference on Computer Modelling and Simulation. pp. 289–294.

Zhang, Y.C., 1991. Complexity and 1/f noise. a phase space approach. Journal de Physique I 1, 971–977.

Zunino, L., Ribeiro, H., 2016. Discriminating image textures with the multiscale two-dimensional complexity-entropy causality plane. Chaos, Soliton and Fractals 91, 679–688.

Zunino, L. Soriano, M., Ribeiro, H., 2012. Distinguishing chaotic and stochastic dynamics from time series by using a multiscale symbolic approach. Physical Review E 86, 046210.

Declaration of interests

☒ The authors declare that they have no known competing financial interests or personal relationships that could have appeared to influence the work reported in this paper.

☐ The authors declare the following financial interests/personal relationships, which may be considered as potential competing interests:

Conflict of Interest: The authors declare that they have no conflict of interest.

Cristina Morel